Structural monitoring of a highway bridge using passive noise recordings from street traffic

Johannes Salvermoser and Céline Hadziioannou[a)]
Department for Earth and Environmental Sciences, Ludwig-Maximilians-University, Theresienstrasse 41, 80333 Munich, Germany

Simon C. Stähler
Leibniz-Institute for Baltic Sea Research, Seestrasse 15, 18119 Rostock, Germany

(Received 27 February 2015; revised 6 November 2015; accepted 28 November 2015; published online 24 December 2015)

Structural damage on bridges presents a hazard to public safety and can lead to fatalities. This article contributes to the development of an alternative monitoring system for civil structures, based on passive measurements of seismic elastic waves. Cross-correlations of traffic noise recorded at geophone receiver pairs were found to be sufficiently stable for comparison and sensitive to velocity changes in the medium. As such velocity variations could be caused by damage, their detection would be valuable in structural health monitoring systems. A method, originally introduced for seismological applications and named Passive Image Interferometry, was used to quantify small velocity fluctuations in the medium and thereby observe structural changes. Evaluation of more than 2 months of continuous geophone recordings at a reinforced concrete bridge yielded velocity variations $\Delta v/v$ in the range of -1.5% to $+2.1\%$. The observed fluctuations correlate with associated temperature time series with a striking resemblance which is remarkable for two completely independent data sets. Using a linear regression approach, a relationship between temperature and velocity variations of on average $0.064\%\ ^{\circ}C^{-1}$ can be identified. This value corresponds well to other studies on concrete structures.
[http://dx.doi.org/10.1121/1.4937765]

[RKS] Pages: 3864–3872

I. INTRODUCTION

Large-scale structures, especially heavily used ones like bridges, operate over decades until eventually their capacity and reliability expires. For cost minimization reasons, most operators try to run the structures as long as possible. Since failure would result in high damage to lives and property, this is only possible with a reliable monitoring system in place. The most common technique for monitoring is regular visual inspection of the structure combined with localized nondestructive measurements. Since this kind of inspection is expensive and personnel-intensive, their rate is very limited, mostly to once a year or less. Moreover, they concentrate on typical points of failure, such as the casing of tendons and places where run-off water from the street can cause chemical degradation of the concrete via the alkali-silica reactions (ASRs). Therefore, global monitoring techniques, where a small set of measurements would allow to check the overall state of a structure at once, are extremely promising.

One candidate is modal measurements, which aim to detect perturbations of modal parameters (natural frequencies, modal shapes) caused by structural changes. These have first been used in combination with active vibration sources, often in big monitoring campaigns on bridges and dams. Due to the enormous logistical effort and poor temporal resolution of active (input–output) measurements with large vibration sources, recent studies also employ ambient vibrations (output-only).[1] New, more sensitive transducers and A/D converters make it possible to extract information from smaller, traffic- and wind-induced vibrations.

Increasing computational power allows to simulate damage scenarios on more and more complex structures. Using finite element (FE) models and damage detection algorithms improves "automated" structural health monitoring (SHM).[2–4] Unfortunately, the underlying FE models are usually only an incomplete representation of the structure and environmental effects, especially temperature variations, are hard to gauge. This affects the overall reliability of automated SHM methods dealing with modal parameters.

Time-domain based approaches like the ultrasonic (US) pulse velocity method have many applications in small-scale testing.[5] Laboratory experiments on concrete samples[6–8] have shown that weak changes in material properties (caused by stress or temperature variations) can be detected by measuring multiply scattered waves (pulse), emitted by a kHz-source, at a nearby receiver. One of the authors of this paper measured stress variations in a concrete bridge using multiply scattered waves around 1 kHz. However, correcting for disturbances caused by fluctuating environmental conditions is still complex.[9] In addition, the wave propagation distance is limited to a few meters in most applications and many repeated measurement campaigns would be needed to achieve a sufficiently high temporal resolution for monitoring.

The idea of monitoring small changes in material properties with passive signals was adapted from seismology. The Green's function between two receivers can be retrieved from diffuse wavefields (e.g., ambient noise) recorded at the

a)Electronic mail: hadzii@geophysik.uni-muenchen.de

receivers.[10] For uniformly distributed noise sources and long records, the cross-correlation between the noise records converges toward the Green's function, which contains all the information about the medium in between. This principle also holds for seismic noise, if cross-correlations are averaged over sufficiently long periods (weeks to months).[11] A couple of studies have been using the noise correlation method in combination with coda wave interferometry (CWI) to monitor changes in seismic velocity. The method is now known as Passive Image Interferometry (PII),[12] and we will refer to it as such in the remainder of this article. PII, which is further explained in Sec. II, was subsequently used to monitor fault zones[13] and active volcanoes.[14]

This study aims toward the development of a passive time-domain technique for the monitoring of civil structures. It applies the seismological method of PII to small scales. To that end, 27 geophones were installed in the girder of a 229 m long highway bridge, and have been recording the vertical motion of the bottom slab continuously (Sec. III). The main observation is that the recorded signal is dominated by traffic induced noise and that the strongest peaks come from cars crossing the extension gap at either end of the bridge (Sec. III B). Section IV explains how that signal can be used for PII. The results, presented in Sec. V, show that the temperature signature on the elastic wave velocities can be measured efficiently with PII using traffic noise. This is promising, as it means the method of PII could be applied to a range of structures where strong cultural noise sources, like car traffic, are available. Our results have been tested for biases caused by temperature sensitivity of the sensors in Sec. VI A and compared with prior studies using active measurements on bridges and in the laboratory in Sec. VI B. The discussion concludes with an examination of the relation between temperature and velocity changes (Sec. VI C).

II. METHOD

A. CWI

The CWI allows to extract changes in wave propagation speed.[15] Measuring velocity changes by using the travel time differences of direct wave arrivals has a limited resolution. However, for a given homogeneous wave speed change, the travel time delay dt will increase linearly with lapse time.[16] CWI takes advantage of this fact by measuring the shift of a whole wave-train at the late part of a seismic signal which consists of scattered wave arrivals, and is named the *coda* (cf. Fig. 1). By doing so, CWI enables an exact measurement of small relative travel time changes, as the absolute changes accumulated in the seismic coda are larger. Moreover, by considering changes in individual wiggles in the coda, it could be possible to detect changes in the scatterer distribution.[17,18] A relative velocity change $\Delta v/v$ is related to a relative travel time change $\Delta t/t$ in the medium. Assuming a mostly homogeneous travel time ($\triangleq$ velocity) change $\Delta t/t = \epsilon$ in the medium, we expect to observe a perturbed time series $h'(t)$:

$$h'(t) = h(t(1-\epsilon)). \tag{1}$$

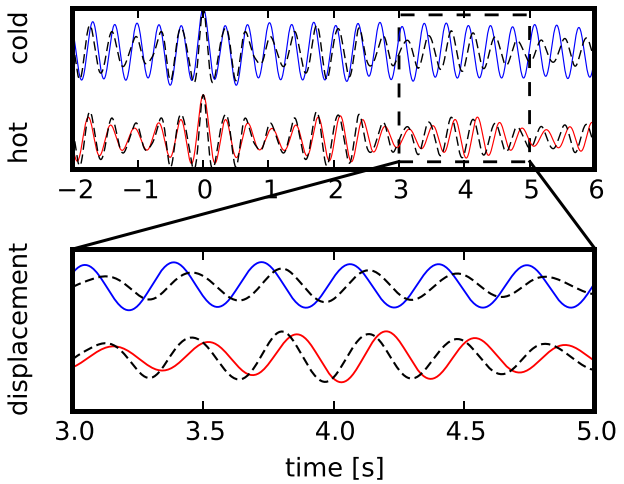

FIG. 1. (Color online) Real data example for extreme temperature cases; "cold" (blue): cross-correlation of 1 h of noise recorded at two receivers at a temperature of −23 °C, "hot" (red): same for temperature of +13 °C, black dashed line: reference signal consisting of the average of all cross-correlations from the total recording time. The signal recorded on a cold day is clearly compressed compared to the reference, the signal corresponding to a hot day is stretched. The displacement amplitudes are normalized.

This effect can be quantified by means of the stretching method.[12,19]

From Eq. (2), we obtain a correlation coefficient (CC) that represents a measure of similarity for a certain window $t \pm T/2$ and a stretching factor ϵ. The signal $h'(t)$ is stretched by different values of ϵ to fit it to the reference trace $h(t)$. The best fitting velocity change (grid search optimization) is found at the ϵ for which CC reaches a maximum.

$$\mathrm{CC}(\epsilon) = \frac{\int_{t-T/2}^{t+T/2} h'[t(1-\epsilon)]h[t]dt}{\sqrt{\int_{t-T/2}^{t+T/2} h'^2[t(1-\epsilon)]dt \cdot \int_{t-T/2}^{t+T/2} h'^2[t]dt}}, \tag{2}$$

where $h(t)$ is the reference correlation function (RCF), $h'(t)$ is the variable function (CCF), ϵ is the stretching factor ($= \Delta v/v$), t is the lapse-time, and T is the length of the lapse-time window.

B. Application to noise cross-correlation

In order to obtain repeatable signals, we use the noise correlation method. The correlation of uniformly distributed noise, recorded at two receivers over a sufficiently long period, converges toward the Green's function between those receivers.[11,20] Since the Green's function contains all information about elastic parameters, comparing the Green's functions calculated at different times allows to detect and characterize changes in these parameters.[12] Changes in the elastic parameters could be caused by varying internal stress states, temperatures, or structural damage.

The method should work even for short noise durations. While the cross-correlated function (CCF) might not have converged to the Green's function, it can still be used to detect temporal changes.[21] If the correlations are sufficiently

stable, complete convergence is not necessary to monitor velocity variations. In our case, hourly CCFs have been found to be sufficiently stable for comparison and sensitive to velocity changes in the medium.

In the following, we measure velocity changes caused by the temperature variations in a reinforced concrete bridge. Temperature variations most likely have a homogeneous effect on seismic velocity in our measurements due to their slow and even propagation into the bridge material. In this case, the shape of the coda is preserved due to a stable scatterer distribution and therefore the linear relation $dv/v = -dt/t$ applies.

III. MEASUREMENT SETUP

A. Setup

To record traffic noise, 27 standard geophones ($f_{corner} = 4.5$ Hz, $R_{coil} = 380\ \Omega$) were installed on the same bridge as has been used in an earlier study about stress variations.[9] To protect the instruments from the weather, they were installed on the bottom slab of the accessible box girder below the deck slab [see Fig. 2(b)]. To ensure constant coupling, they were fixed by cementing them to the concrete [Fig. 2(d)]. From the eastern end of the bridge, the array with a spacing of 4 m extends 100 m toward the center of the 229 m long bridge [Fig. 2(a)].

The bridge supports a road with two traffic lanes, one for each direction. It is not fixed at the ends to allow for length variations caused by thermal expansion. Thus, expansion joints can be found at both ends of the bridge. Since the Steinachtal bridge is a rather recent construction (*2008), we do not expect damage to interfere with our measurement. More characteristics can be found in Table I. Ambient noise generation on this bridge is supposed to be primarily driven by traffic. Vehicles passing the expansion joints produce blasts that excite different waves with a broad spectrum. Compressional waves have the highest velocities and frequencies. However, since their wavelength is large compared to the width of the deck slab, only very high frequencies ($\gg$ 10 kHz) can propagate freely. At these frequencies, which are outside the range of our instrument sensitivity, attenuation becomes dominant. Therefore, we concentrate on longer period flexural waves of the whole superstructure. These propagate back and forth between the ends of the bridge after excitation. A correlation of the recordings between each pair of receivers on the bridge is adequate, as the direct and flexural waves are always recorded by both of them.

In two measurement periods (December 21, 2011–January 14, 2012 and February 1, 2012–March 10, 2012), traffic noise has been recorded by the geophone array at a sampling frequency of 500 Hz. The traces of all geophone-channels were continuously stored in SEG2-format streams of 32 s length.

Two sets of temperature data are available for evaluation of the temperature effect on the Steinachtal bridge. One detailed set is available for 2011, corresponding to the first 10 days of measurement. It contains 2 temperature time series at the surface of the road and at 30 cm depth inside the concrete deck slab. A second set of temperature measurements from the meteorological station Kronach, about 10 km away, was obtained from the German Meteorological Service (Deutscher Wetterdienst). We obtained air-temperature data with an hourly resolution that was measured 5 cm above the ground, which came closest to the conditions on the bridge. Apart from slightly lower fluctuation amplitudes in the in-bridge data, the agreement between the measurements of the two sites was surprisingly good.

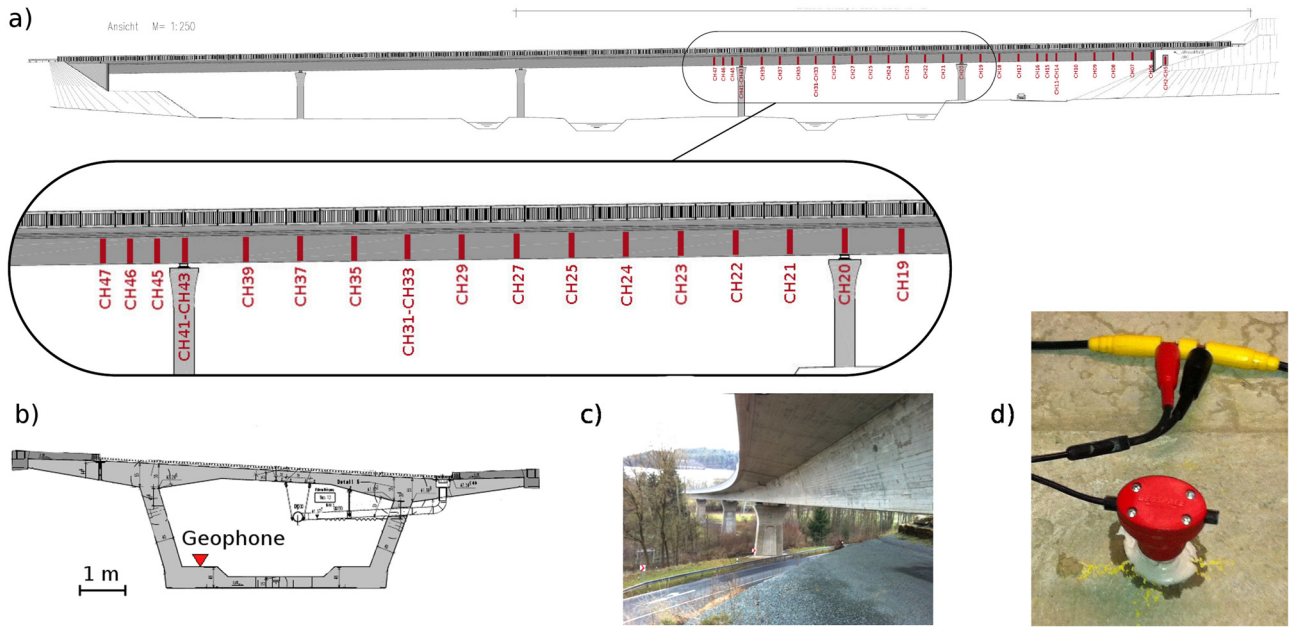

FIG. 2. (Color online) (a) Lateral view on the 229 m long Steinachtal bridge (scheme) looking north-ward. Bars indicate the positions of geophones in the box girder. (b) Cross-section of the box girder with geophone position indicated by a triangle. (c) The photo shows the bridge in construction state, viewed from below. (d) Attachment of a geophone to the bridge. The instrument was screwed on a footplate slab, which was then cemented onto the bridge. It was not possible to drill holes into the bridge itself.

TABLE I. Characteristics of the bridge.

Steinachtal bridge	
Coordinates	N50° 12′50″ E11° 13′13″
Length	229 m
Distance between supports	42.5-48-48-48-42.5 m
Width of deck	12.00 m
Width of base plate	5.00 m
Thickness of deck	0.25 m
Traffic volume	10–200 vehicles/hour

B. Signals

Typically, the traffic-noise recordings feature rather flat background noise and a number of distinct peaks depending on traffic activity. As mentioned before, these peaks are produced by vehicles passing the bridge. Their occurrence rate depends on the traffic volume which is especially high during rush hours and low between midnight and 4 a.m.

A priori, it was unproved whether we can use signals that are corrupted by traffic noise or not. Hence, in the following we have conducted an automated separation between "calm" and "noisy" traces to evaluate them separately. In this context calm means no vehicle passed the bridge in the 32 s time window and noisy means that passing vehicles led to distinct peaks in the seismograms. Eventually, using the noisy traces turned out to be necessary because of the poor temporal coverage by the calm traces.

A closer look at the single events reveals that they are not simply uniform peaks, but clearly display notable features (Fig. 3). Aside from the fact that one event lasts for 20–30 s, there is a clear onset and a fading out over several seconds at the end. Two distinct peaks can be found in the spectrogram of Fig. 3. They are related to high amplitude direct waves produced by the vehicle passing the expansion gaps on either end of the bridge. We can also observe slowly decaying amplitudes following the second hit. These also appear in the spectrogram, but such that high frequency amplitudes decay much faster than lower ones. Low frequencies are associated with flexural waves (reverberations) propagating back and forth between the unbound ends of the bridge.

In Fig. 3(b), the horizontal, permanently excited frequency bands at 12.5, 50, 100, and 150 Hz are most likely related to electro-magnetic (e-m) noise induced by a power line crossing the bridge.

The unfiltered spectrum (Fig. 4) shows 5 higher peaks between 2 and 6 Hz, likely associated with natural frequencies of the bridge.

We concentrate here on the frequency band containing the bridge's natural frequencies and the long lasting, low-frequency reverberations, i.e., 2–8 Hz.

IV. PROCESSING

Here we will use noise cross-correlation as explained in Sec. II B. In our experiment, the seismic waves are excited primarily at the two ends of the examined bridge, propagating unilaterally along its horizontal axis. The setup is suitable to compute CCFs of receivers along this axis; nevertheless it does not correspond to a uniform source distribution as required for Green's function retrieval, by definition. This section shows how we prepare appropriate CCFs that capture the environmental conditions of the bridge regardless and how these are employed to uncover small changes in seismic velocity.

Most of the processing is done with toolboxes of ObsPy[22] and NumPy.[23,24]

A. Filtering and cross-correlation

After de-trending, the data are pre-filtered to a 2–8 Hz band using Butterworth zero-phase filters.

Our main interests are reverberations of natural frequencies and their overtones as they are stable and persistent. As a tool to remove non-stationary events in seismic records, one-bit normalization[25] is suitable to diminish the impact of direct surface waves on cross-correlations by decreasing their distinctive amplitudes. The one-bit cross-correlation C^{ob}_{AB} is defined as:

$$\mathrm{CCF}^{ob}_{AB}(t) = \int \mathrm{sgn}[A(\tau)] \cdot \mathrm{sgn}[B(t+\tau)]d\tau, \tag{3}$$

where $A_p(\tau)$ and $B_p(\tau + t)$ denote the signals from a point source P recorded at the receivers A, B.

Our correlation functions are produced by first merging the 32 s records to 2-min signals, calculating the CCFs and stacking about 30 of these to hourly stacks.

In order to evaluate the stability of the resulting CCFs, we calculate the signal-to-noise ratio (SNR) as follows [Eq. 4)]:

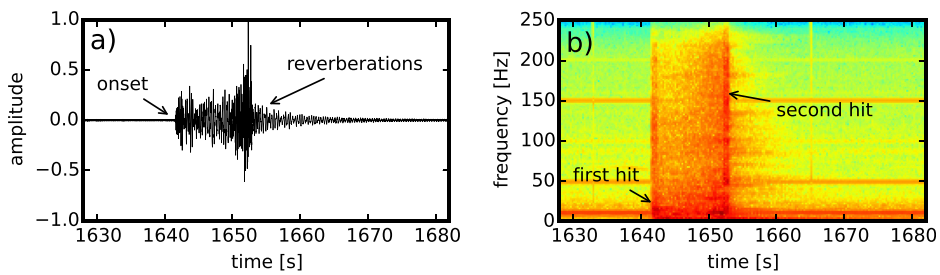

FIG. 3. (Color online) (a) Waveform recorded for a car passing over the bridge and (b) spectrogram for this event. Characteristic features of this signal are two clear onsets (corresponding to the vehicle passing the expansion gap at either end of the bridge) and distinct reverberations. The amplitudes suggest that the car passed the more distant extension gap first, i.e., that it was traveling east-ward [compare Fig. 2(a)]. The time difference of roughly 10 s between the crossings of the two gaps correspond to a car velocity of roughly 80 km/h, which is indeed the local speed limit.

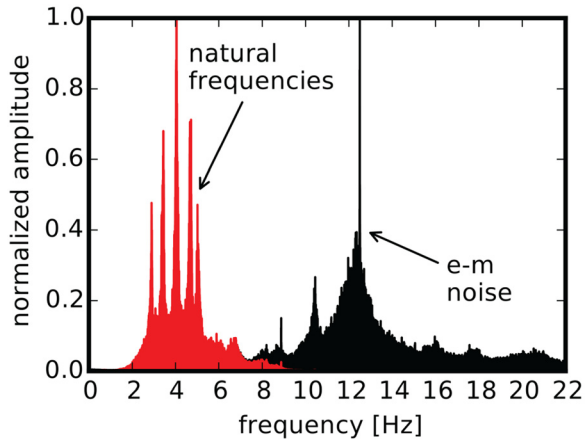

FIG. 4. (Color online) Normalized spectrum for 6 h of traffic noise recorded at a single geophone. The measurement was not corrected for instrument response, which explains the drop below 2 Hz. The peak at 12.5 Hz is constant over the whole measurement period, while the peaks between 2 and 5 Hz vary slowly over time. Indicated are the natural frequencies of the bridge and an e-m noise band caused by a power line crossing the bridge. The black unfiltered spectrum is overlain with the filtered spectrum (red) that is used in our analysis.

$$\mathrm{SNR} = \frac{\max\left(|\mathrm{CCF}(t)|\right)}{\mathrm{std}(\mathrm{CCF}(t))}. \tag{4}$$

As more 2-min CCFs are stacked, the SNR increases. From this analysis, we have concluded that 1 h long CCFs (SNR $\geq$ 4000) are stable and reproducible enough for further use.

Several methods have been proposed to determine velocity changes in media from CCFs. In the case of PII,[12] the stretching method has proven to be adequate. As described in Eq. (2), our hourly CCFs are compared to a RCF. In our case the RCF is represented by a normalized stack of all hourly CCFs for the receiver pair (e.g., RCF for CH27–CH37). More than 30 receiver pairs with different inter-receiver distances (4–90 m) and locations on different sections of the bridge have been tested in this analysis.

B. Effect of temperature changes

Our main focus is the observation and evaluation of temperature induced velocity changes. The general assumption is that wave velocities decrease with increasing temperature in the medium, thus the travel time of the waves increases. This is caused by an alteration of the elastic moduli (Young's Modulus, etc.) that also affect the propagation of seismic waves. All elastic parameters must be considered temperature dependent. Additionally, thermal expansion will affect our measurements. This effect is separately discussed in Sec. VI A.

Figure 1 illustrates differences in CCF waveform traveltimes for two extreme cases of high and low temperature regime extracted from our measurements. When compared to the reference function, either the CCF is compressed (cold) or stretched (hot). Figure 1 also clarifies why we examine the coda of the CCF and do not investigate the first arrivals: the effect increases the longer the wave is traveling in the medium (longer wave paths) and thus the later in the CCF.

The time window we use for our analysis extends from 0.05 to 11.5 s in the causal part (positive lapse times) of the CCF. The part before 0.05 s is skipped to avoid the direct arrivals at all receivers and the 11.5 s limit corresponds to a minimum 75%-decay time for the CCFs, after which the waveforms become less deterministic.

V. RESULTS

The evaluation of velocity changes caused by temperature fluctuations on the bridge yields interesting results.

As described in Sec. II, we use the stretching method to measure relative wave speed changes $\Delta v/v$. Most of the associated CCs are larger than 90%, decreasing slightly during low-traffic periods at night and rising to peaks of 99% at the daily rush hours.

We discovered a striking resemblance between the resulting curve of velocity variations over time and the time series of temperature measurements for the same period as seen in Figs. 5 and 6. Here, instead of $\Delta v/v$ we display $\Delta t/t = -\Delta v/v$ to more easily compare the shape of the velocity variations curve with that of the temperature values. For increasing temperatures, we observe increasing travel time delays, i.e., decreasing velocities.

When considering the trends of both curves in the figures, one recognizes a constant time shift between the two measurements that is probably related to thermal diffusion. Since we measure air temperature for this period, there is a natural delay time in which the ambient temperature propagates into the concrete of the bridge where it then induces velocity variations. In this context, time lags on the order of 3 h were observed. This is reconsidered in Sec. VI C. Apart from the time shift, the agreement between these two completely independent measurements is very high. Furthermore, the

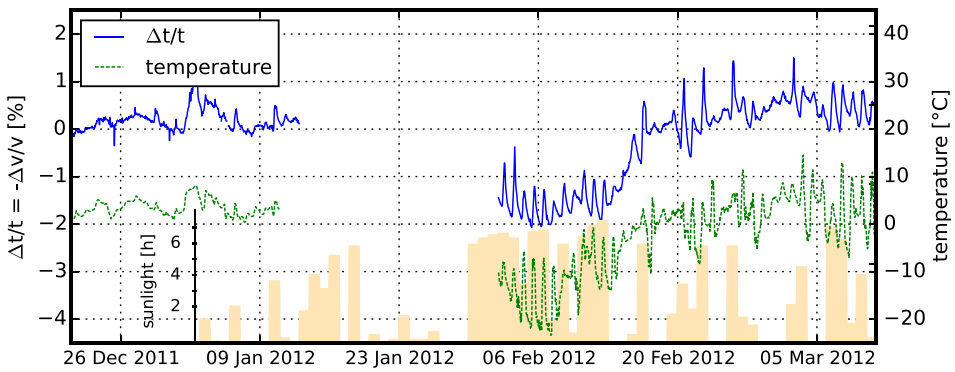

FIG. 5. (Color online) Velocity variations at receivers 35/22 for the complete measurement period. Hours of daily sunlight (bar plot) and temperature (dotted line) are plotted to emphasize their importance as environmental factors influencing the seismic velocity on the Steinachtal bridge. It can be seen that sunny days have higher amplitude fluctuation in the diurnal velocity variations. This may be explained by stronger temperature gradients in the concrete due to surface heating by direct solar irradiation.

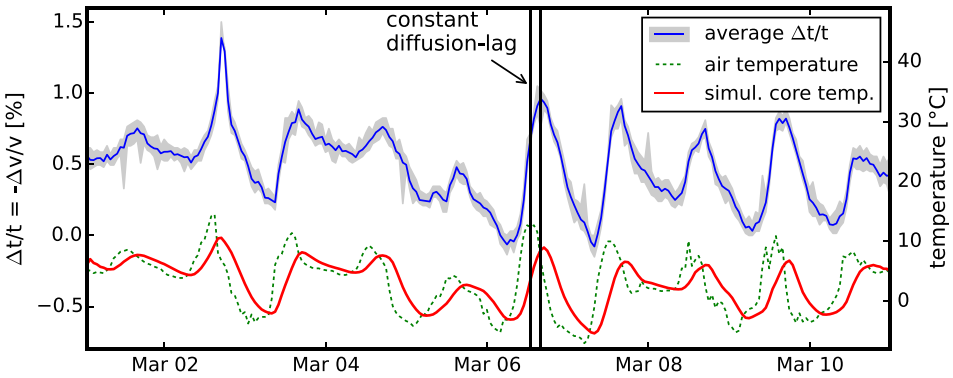

FIG. 6. (Color online) Relative velocity variations of the first days of March, averaged over 32 receiver pairs, where only velocity variations corresponding to CCs ≥ 0.85 are considered. The shaded area indicates the standard deviation of the velocity variation curve. The air temperature is shown with a dotted line, while the vertical lines show the constant thermal diffusion lag of about 3 h. This shift also fits the simulated core temperature (solid line), assuming a slab-width of 36 cm VI C.

different receiver pairs (32 overall) we have tested show very similar results, as can be seen from the small variance around the average velocity variation curve in Fig. 6.

Considering the results of different parts of the measurement period, we discovered clear differences in their patterns. For December 2011 and January 2012, the velocity variations are not dominated by daily cycles but by a rather flat long-term evolution. In contrast, February and March 2012 show distinct daily fluctuations in both temperature and velocity variations.

Figure 5 reveals that this is a meteorological issue. Environmental data were recorded by instrumentation installed permanently on the bridge for road condition monitoring. These were compared to our measurements. The difference in the variation pattern seems to be related to cloud cover or rather daily hours of sunlight, which are plotted in Fig. 5 for comparison. High temperature fluctuations naturally correlate with more hours of daily sunlight (increased heating) combined with a clear sky during the night, causing stronger ground cooling then.

Further investigations were performed with regard to other environmental effects and their influence on relative velocity variations. We found that neither humidity of the road, nor precipitation itself, nor wind speed (peak or average), feature any correlation with the observed patterns.

For the overall measurement period we obtained relative velocity variations in the range of -1.5% to $+2.1\%$, while air temperature data yields values between $+14\,^{\circ}\mathrm{C}$ and $-23\,^{\circ}\mathrm{C}$.

To numerically quantify the relationship between temperature and velocity change and make our results comparable to prior studies, we estimated relative velocity variation rates (VVRs) with a linear regression approach (Fig. 7). We fitted temperature-velocity-variation pairs with a linear regression each day and inferred the relative velocity variation per $^{\circ}\mathrm{C}$. The quality of this rate was then verified by removing the inferred temperature effect from the original velocity variation curve. To do this, the temperature curve was scaled using the calculated VVR, and subtracted from the velocity changes. Assuming no damage or other effects occurred during the measurement period, this should result in a flat response.

For short intervals, up to 24 h, this method worked reasonably well, yet for longer intervals the subtraction did not result in a flat response. One of the reasons for this is that the effect of temperature on velocity in the bridge is presumably non-linear. The VVR varies over a range of values depending on the temperature. Potential explanations for this behavior are reasoned in Sec. VI C.

VI. DISCUSSION

In an experiment covering more than 2 months of recording on the Steinachtal bridge, long-term trends and daily variations of temperature could be clearly traced by means of velocity variations.

A. Reliability tests

The results presented in Sec. V were tested for plausibility regarding different physical effects that could affect the outcome.

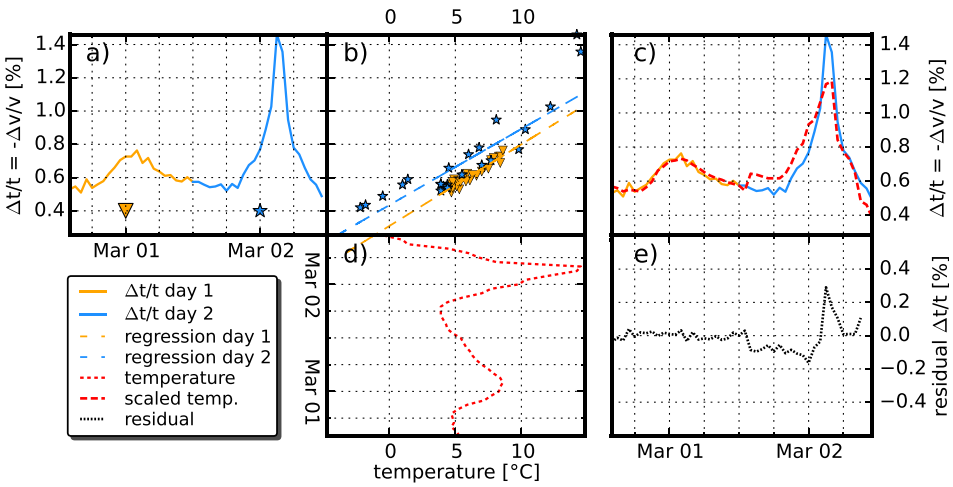

FIG. 7. (Color online) Linear regression for temperature compensation: (a) Velocity variations as in the other figures plotted as $\Delta t/t = -\Delta v/v$ for two days, March 1 (triangle) and March 2 (star), (d) temperature series for the same period, shifted by -3 h to account for thermal diffusion, (b) velocity variations plotted against temperature, linear regression for each day separately, (c) velocity variations and scaled temperatures, using regression parameters from (b), and (e) residual after subtracting the curves of (c), i.e., temperature effect reduced.

First of all, the impact of thermal expansion was considered: a lower density for higher temperatures is equivalent to an increase in volume. In other words, as temperatures fluctuates the bridge experiences thermal expansion. However, engineering studies[26] state that the effect is small, with a linear expansion coefficient α on the order of $6 - 14 \cdot 10^{-6}\,(1/K)$. Therefore, associated variations in length are orders of magnitude too small to explain the observed wave speed fluctuations.

The impulse response of the geophones could be affected by temperature variations as well. The corner frequency of the devices can shift as a result of temperature change, which can generate significant phase shifts. This would produce delays in the seismogram that could be misinterpreted as velocity variations in the medium. In order to assess whether a change in instrument response could indeed be responsible for our observed changes in wave speed, we perform a synthetic test. We use a signal recorded by one of the geophones, and deconvolve the instrument response. Then, the signal is convolved with another, artificial response. This artificial response is modified in such a way that the corner frequency is shifted to simulate a temperature induced shift and deliberately introduce a delay.

We have tested the impulse response for shifts in corner frequency up to the unrealistic maximum of 10 Hz as a precaution. However, even such an extreme shift only produces an apparent relative delay on the order of 0.52%, while our measurements encountered relative velocity variations larger than 3%. We can therefore exclude that changing instrument responses severely contaminate our measurements.

B. Comparison with prior studies

In order to further check the validity of our evaluation, we draw a comparison to the findings of prior studies. In this case, problems for direct comparability of different studies arise from the various temperature and frequency ranges that were used as well as the differences in sizes of the investigated samples. These issues possibly involve discrepancies in material behavior, i.e., caused by temperature gradients (size), multiple scattering (frequency), and source distribution (geometry). Table II summarizes the findings of previous studies and of this study.

It is important to note that the experiments mentioned below were using small-scale bodies under laboratory conditions with well-known sources. The active vibration sources they used are in the kHz-range, therefore multiple scattering plays a role in their analysis.

In earlier studies about vibrations in kHz range,[5,6] comparatively high VVRs of 0.15%/°C, respectively, 0.16%/°C were proposed, but in a temperature range (26 °C–30 °C) outside that of our experiment. Assuming that the VVR is not implicitly linear (see our min. and max. values in Table II), a comparison between the outcomes is not flawless.

While also in these authors' experiment, a concrete slab was heated unilaterally by the Sun,[6] a concrete slab that was heated unilaterally by the Sun, for our experiment we can assume a more uniform temperature distribution in the medium. Nevertheless, different materials were involved (asphalt covering, concrete, etc.) which behave differently to effects of, e.g., insulation and moisture. Especially the blacktop of the road exhibits temperature dependent properties. While for temperatures $\geq$0 °C it is flexible, below freezing temperatures it contributes considerably to the stiffness of the structure.[28] It therefore affects physical properties associated with wave velocity, potentially causing non-linearities in the VVRs.

This behavior, among other factors, can partly account for the variable VVRs we observed (Sec. V), and makes clear why different structures should be treated independently.

Another small-scale study[7] observed a drop in US pulse velocity of 2%–3% for an increase in temperature from 0 °C to 50 °C. This results in a smaller VVR (≈0.06%/°C) compared to the concrete slab experiment[6] discussed above, if linear behavior is assumed. The obtained range is more similar to our outcome.

The authors investigated C30/37 (=concrete composition) concrete prisms of $10 \times 10 \times 30$ cm size. CWI combined with high frequency waves (multiple scattering) allowed them to sample the entire blocks. They had to deal with permanent changes after their first heating/cooling cycle, which were attributed to aging effects or moisture issues. Again, this proves how the obtained results are influenced on environmental conditions even when evaluating the same body.

Generally, determining a specific calibration factor or pattern to subtract the temperature's effect from velocity changes in an arbitrary structure is problematic. We attempted to eliminate the temperature overprint as described in Sec. V, by determining the VVR and using it to scale and subtract temperature data. This is our first step toward the removal of temperature effects, with the aim to improve the discrimination between harmless temperature- and damage-induced deviations. Furthermore, we might be able to recognize gradual changes in the observed VVRs, which could be associated with long-term settling or degradation by ASR, carbonation, and others. Future studies, with more accurate temperature measurements and long-term instrument installations ($\geq$1 yr)

TABLE II. Results of our and prior studies in comparison. Note the differences in sample size, frequency range, etc., which potentially affect the outcomes.

Publication	Sample size	Freq.-range	Temp.-range	VVR	Rel. Vel. Variation
This study	$94 \times 12 \times 0.5$ m	2–8 Hz	−23 °C to +14 °C (air temperature)	min. $\frac{0.024\%}{°C}$ max. $\frac{0.14\%}{°C}$	−1.5% to +2.1%
British Standard BS1881 (1986) (Ref. 27)	—	0.5–20 kHz	−4 °C to +60 °C	—	−1.5% to +5%
Larose *et al*. (2006) (Ref. 6)	$12 \times 5.5 \times 0.2$ m	1 kHz	+26 °C to +30 °C	$\frac{0.15\%}{°C}$	–
Niederleithinger and Wunderlich (2013) (Ref. 7)	$0.1 \times 0.1 \times 0.3$ m	55 kHz	0 °C to +50 °C	—	decrease by 2%–3%

at their disposal, are needed to improve the compensation of environmental overprints.

C. Temperature effect

A matter to be clarified is by which process the temperature actually affects the wave velocity in the medium. We have performed a simple one-dimensional diffusion simulation to investigate that issue. An explicit finite differences scheme, employing a thermal diffusivity of $10^{-6}\,m^2/s$ and a typical slab thickness of 36 cm, yields the "simulated core temperature" in Fig. 6. This core temperature curve highly correlates with the velocity variation series by means of shape and is shifted compared to the air temperatures. Thereby, we confirmed that the time lag of about 3 h is plausibly explained by thermal diffusion and that, to first order, the velocity variations are linked to the core temperature of the bridge. However, we see in Fig. 7 that for different temperature patterns, e.g., fast vs slow increase, we observe diverging VVRs, and thus a difference in system response to these features. From that, we may argue that temperature gradients still play a role in the evolution of the shape of the velocity variation curve and must be considered when eliminating the temperature effect.

VII. CONCLUSIONS

Due to increased safety norms and aging structures, the interest in performing SHM is steadily growing. Different approaches for SHM have been proposed in the last decades to replace the well-established but sometimes unreliable visual inspection. Important features for future systems are improved temporal resolution, higher accuracy, and lower logistical effort. Consequently, passive monitoring techniques are appropriate to fulfill these requirements.

Damage is often indicated by deviations of wave velocity in the medium caused by opening cracks, loss of prestress, or other disturbed scatterer distribution. Our aim was to extract relative velocity variations using a technique called PII and to apply this to a small-scale environment. PII is based on the comparison of stable cross-correlation functions (CCF)—ideally Green's functions (GF) that require a uniform noise source distribution. In our experimental setup, we dealt with uniaxial noise sources, and therefore did not measure proper GFs. Instead, we have shown that it is possible to obtain stable cross-correlation functions for receiver pairs. These CCFs are sufficiently sensitive to changes in medium properties[29] and approximate GFs to a great extent in our application.

As a case study, 27 geophones were installed on a highway bridge. These geophones were left to continuously record background noise—mostly generated by traffic—for a duration of approximately 2 months. High traffic activity produced highly stable and reproducible CCFs, in which most of the bridges' natural frequencies were excited between 2 and 8 Hz. By comparing hourly CCFs with an all-time average reference stack via the stretching method, we could show that temperature induced velocity variations can be traced.

The velocity variations $\Delta v/v$ range between -1.5% and $+2.1\%$, corresponding to temperatures ranging from $-23\,^{\circ}C$ to $+14\,^{\circ}C$ (see Table II). In a comparison with previous studies, we ascertained that our observed values are on the same order of magnitude.

Comparing the two resulting time series (temperature and velocity variation, Fig. 6) over the time intervals yielded a strong resemblance. The temporal delay of a few hours between the corresponding values of temperature and velocity variation is associated with thermal diffusion, while velocity variation patterns seem to be linked to temperature gradients as well.

Due to the strong conformity of the two completely independent measurements, we have proceeded with an estimation of a scaling factor between temperatures and wave velocity changes, a VVR per °C. In a linear regression approach to adjust temperature values to velocity variations for each 24 h-interval consecutively, we calculated the best fitting VVRs. Although we observe temperature dependent variation rates (average: $0.064\%/\,^{\circ}C$), the subtraction of the measured velocity variation and adjusted temperature series in 24 h-intervals yield an almost flat and theoretically temperature independent velocity variation residual. That confirms the validity of the calculated VVR, and represents a first approach to reduce an environmental effect to thereby accentuate damage induced variations on the structure. Considering very long-term measurements, even a gradual change in VVR (-range) could indicate structural changes due to damage or aging.

Our method features some advantages in the context of SHM. These are high temporal resolution ($\leq$1 h) and continuous applicability with minimal logistical effort and at relatively low cost. Furthermore, we reach good accuracy in determining relative velocity variations and are able to adequately subtract the temperature effect on seismic velocities in the medium.

However, improvements in temperature elimination could be gained by having access to more suitable and extensive temperature measurements inside the bridge, for example, between asphalt layer and concrete slab.

The main drawback associated with low frequencies and late-coda analysis is poor spatial resolution. While we are able to recognize minimal velocity changes at high temporal resolution, it would be difficult to localize their exact origin. Nevertheless, the passive method proposed in this paper could be imagined as a permanent monitoring and early-warning system. The detection of a velocity change would give rise to a visual inspection including punctual tests via US pulse methods or, e.g., ground-penetrating radar. In the future, it would be reasonable to perform further experiments that include real damage scenarios to evaluate the sensitivity of our method to damage induced velocity variations. In the course of such an experiment, a cross-check with other methods (US, modal analysis, etc.) could offer valuable clues and help to develop a continuously working monitoring system for civil structures.

ACKNOWLEDGMENTS

We would like to thank the Karlsruher Institut für Technologie (KIT) for providing the geophones and other

equipment. We thank the Autobahndirektion Nordbayern for allowing us to perform measurements on the Steinachtal bridge and for providing access to temperature measurements. We thank the engineering company Stähler and Knoppik for providing the building plans. We want to express our gratitude to field workers Namat Amat, Stefan Wenk, Kasra Hosseini, and Tobias Megies who helped install the instruments and to Christoph Sens-Schönfelder, Ernst Niederleithinger, Roel Snieder, and Eric Larose for inspiring discussions. This project was partially funded by the Emmy-Noether Program of the DFG (Project No. HA7019/1-1). We thank two anonymous reviewers for their constructive comments.

[1]Á. Cunha and E. Caetano, "Experimental modal analysis of civil engineering structures," Sound Vib. **40**, 12–20 (2006).
[2]F. Magalhães, A. Cunha, and E. Caetano, "Vibration based structural health monitoring of an arch bridge: From automated OMA to damage detection," Mech. Syst. Signal Pr. **28**, 212–228 (2012).
[3]C. Rainieri and G. Fabbrocino, "Automated output-only dynamic identification of civil engineering structures," Mech. Syst. Signal Pr. **24**, 678–695 (2010).
[4]F. Ubertini, A. L. Materazzi, C. Gentile, and F. Pelliccia, "Automatic identification of modal parameters: Application to a reinforced concrete arch bridge," in *Proceedings of the 5th European Conference on Structural Control*, Genova (2012).
[5]T. Planès and E. Larose, "A review of ultrasonic Coda wave interferometry in concrete," Cem. Concr. Res. **53**, 248–255 (2013).
[6]E. Larose, J. de Rosny, L. Margerin, D. Anache, P. Gouedard, M. Campillo, and B. van Tiggelen, "Observation of multiple scattering of kHz vibrations in a concrete structure and application to monitoring weak changes," Phys. Rev. E **73**, 016609 (2006).
[7]E. Niederleithinger and C. Wunderlich, "Influence of small temperature variations on the ultrasonic velocity in concrete," AIP Conf. Proc. **1511**, 390–397 (2013).
[8]A. Grêt, R. Snieder, and J. Scales, "Time-lapse monitoring of rock properties with coda wave interferometry," J. Geophys. Res. Solid Earth **111**, 1978–2012, doi:10.1029/2004JB003354 (2006).
[9]S. C. Stähler, C. Sens-Schönfelder, and E. Niederleithinger, "Monitoring stress changes in a concrete bridge with coda wave interferometry," J. Acoust. Soc. Am. **129**, 1945–1952 (2011).
[10]O. Lobkis and R. L. Weaver, "On the emergence of the Green's function in the correlations of a diffuse field," J. Acoust. Soc. Am. **110**, 3011–3017 (2001).
[11]N. M. Shapiro, M. Campillo, L. Stehly, and M. H. Ritzwoller, "High-resolution surface-wave tomography from ambient seismic noise," Science **307**, 1615–1618 (2005).
[12]C. Sens-Schönfelder and U. Wegler, "Passive image interferometry and seasonal variations of seismic velocities at Merapi volcano, Indonesia," Geophys. Res. Lett. **33**, L21302, doi:10.1029/2006GL027797 (2006).
[13]U. Wegler and C. Sens-Schönfelder, "Fault zone monitoring with Passive Image Interferometry," Geophys. J. Int. **168**, 1029–1033 (2007).
[14]F. Brenguier, N. M. Shapiro, M. Campillo, V. Ferrazzini, Z. Duputel, O. Coutant, and A. Nercessian, "Towards forecasting volcanic eruptions using seismic noise," Nature Geosci. **1**, 126–130 (2008).
[15]R. Snieder, A. Grêt, H. Douma, and J. Scales, "Coda wave interferometry for estimating nonlinear behavior in seismic velocity," Science **295**, 2253–2255 (2002).
[16]G. Poupinet, W. L. Ellsworth, and J. Frechet, "Monitoring velocity variations in the crust using earthquake doublets: An application to the Calaveras Fault, California," J. Geophys. Res. Solid Earth **89**, 5719–5731 (1984).
[17]V. Rossetto, L. Margerin, T. Planès, and E. Larose, "Locating a weak change using diffuse waves: Theoretical approach and inversion procedure," J. Appl. Phys. **109**, 034903 (2011).
[18]T. Planès, E. Larose, L. Margerin, V. Rossetto, and C. Sens-Schönfelder, "Decorrelation and phase-shift of coda waves induced by local changes: Multiple scattering approach and numerical validation," Wave Random Complex **24**, 99–125 (2014).
[19]O. I. Lobkis and R. L. Weaver, "Coda-wave interferometry in finite solids: Recovery of P-to-S conversion rates in an elastodynamic billiard," Phys. Rev. Lett. **90**, 254302 (2003).
[20]N. M. Shapiro and M. Campillo, "Emergence of broadband Rayleigh waves from correlations of the ambient seismic noise," Geophys. Res. Lett. **31**, L07614, doi:10.1029/2004GL019491 (2004).
[21]C. Hadziioannou, E. Larose, A. Baig, P. Roux, and M. Campillo, "Improving temporal resolution in ambient noise monitoring of seismic wave speed," J. Geophys. Res. Solid Earth **116**, 1978–2012, doi:10.1029/2011JB008200 (2011).
[22]M. Beyreuther, R. Barsch, L. Krischer, T. Megies, Y. Behr, and J. Wassermann, "Obspy: A Python toolbox for seismology," Seis. Res. Lett. **81**, 530–533 (2010).
[23]P. F. Dubois, K. Hinsen, and J. Hugunin, "Numerical Python," Comput. Phys. **10**, 262 (1996).
[24]S. van der Walt, S. C. Colbert, and G. Varoquaux, "The NumPy Array: A Structure for Efficient Numerical Computation," Comput. Sci. Eng. **13**, 22–30 (2011).
[25]P. Cupillard, L. Stehly, and B. Romanowicz, "The one-bit noise correlation: A theory based on the concepts of coherent and incoherent noise," Geophys. J. Int. **184**, 1397–1414 (2011).
[26]T. Keller and C. Menn, "Dauerhaftigkeit von Stahlbetontragwerken: Transportmechanismen – Auswirkungen von Rissen (Durability of reinforced concrete structures: Transportmechanis- men – effects of cracks)," Technical Report (1992).
[27]British-Standard-Institution, BS 1881, Part 203, Recommendations for Measurement of Velocity of Ultrasonic Pulses in Concrete, London (1986).
[28]B. Peeters and G. De Roeck, "One-year monitoring of the Z24-Bridge: Environmental effects versus damage events," Earthq. Eng. Struct. D **30**, 149–171 (2001).
[29]C. Hadziioannou, E. Larose, O. Coutant, P. Roux, and M. Campillo, "Stability of monitoring weak changes in multiply scattering media with ambient noise correlation: Laboratory experiments," J. Acoust. Soc. Am. **125**, 3688–3695 (2009).